Supporting Information

Crystal Structure of Gluconate Bound Iron(III) Complex: Synthesis, Characterization and Redox Properties of the Complex in Aqueous Solution

Christopher D. Stewart, Hadi Arman, Brenda Benavides, Ghezai T. Musie*

Department of Chemistry, The University of Texas at San Antonio, San Antonio, TX, 78249, United States. E-mail: ghezai.musie@utsa.edu

EXPERIMENTAL SECTION

Synthesis of the Ligand and Metal Complex

Synthesis of *N,N'*-Bis[2-carboxybenzomethyl]-1,3-diaminopropan-2-ol, H_3cdp. To a solution of 2-carboxybenzaldehyde (4.643 g, 30.00 mmol) and NaOH (1.200 g, 30.00 mmol) in 100 ml methanol was added 1,3-diaminopropan-2-ol (1.424 g, 15.00 mmol) in 20 ml methanol. A yellowish mixture obtained and was heated to 60°C while stirring for 4 h. Then the reaction product was cooled in an ice-bath. To the cold solution was added excess $NaBH_4$ (1.50 g, 39.50 mmol) in portions while stirring. The yellow color was slightly discharged. After 30 min 2 ml conc. HCl was added drop wise to destroy the excess $NaBH_4$. Acidification of the solution to about pH of 5 by addition of more HCl resulted in precipitation of a crystalline white solid. The white solid was filtered out from the mother liquor and washed with H_2O and methanol, and dried at 80°C. Yield: 4.95 g (87%). The compound crystallizes with one molecule of water as found from the elemental analysis and was characterized as H_3cdp·H_2O. *Anal. Calcd*. For $C_{19}H_{22}N_2O_5$·H_2O: C, 60.63%; H, 6.43%; N, 7.44%. *Found*: C, 60.25%; H, 6.28%; N, 7.33%. ^{1}H NMR for the sodium salt of the compound (500 MHz, D_2O, 25°C, δ): 7.46 – 7.32 (m, 8H), 3.92 – 3.80 (m, 1H), 2.63 (q, 4H), 2.55 (q, 4H).

Synthesis of *N,N'*-Bis[2-carboxybenzomethyl]-*N,N'*-Bis[carboxymethyl]-1,3-diamino-propan-2-ol, H_5ccdp. To a solution of *N,N'*-Bis(2-carboxybenzomethyl)-1,3-diaminopropan-2-ol, H_3cdp, (3.58 g, 10 mmol) and NaOH (0.80 g, 20.0 mmol) in 50 ml of water was added a solution of iodoacetic acid (4.65 g, 25.0 mmol) and NaOH (1.00 g, 25.0 mmol) in 50 ml of H_2O. The reaction mixture was heated to reflux while stirring. Over a period of 6 h, more NaOH (0.80 g, 20.0 mmol) was added in portions and the pH of the solution was maintained in the range of 10 - 11. The resulting solution was cooled and acidified with conc. HCl to pH of 3 and a white crystalline product was obtained. The crystalline solid was filtrated and washed with H_2O and methanol, and was dried at 80°C. Yield: 5.2 g (95%). The compound was recrystallized with the HCl and was characterized as H_5ccdp·2HCl. *Anal. Calcd*. for $C_{23}H_{26}N_2O_9$·2HCl: C, 50.47%; H, 5.16%; N, 5.12%. *Found*: C,

50.31%; H, 5.50%; N, 5.06%. FTIR (cm-1): ν = 3503(b), 3032(b), 1667(s), 1590(vs), 1562(s), 1440(s), 1392(s), 1264(s), 1160(s), 902(s), 845(s), 788(s). ^{1}H NMR for the sodium salt of the compound (500 MHz, D_2O, 25°C, δ): 7.51 (d, 2H, J = 7.5 Hz), 7.40 (m, 4H), 7.33 (t, 2H, J = 7.5 Hz), 3.92 (d, 2H, J = 13.5 Hz), 3.82 (d, 2H, J = 13.5 Hz), 3.82 (d, 1H), 3.19 (d, 2H, J = 16.5 Hz), 3.10 (d, 2H, J = 16.5 Hz), 2.62 (d, 1H, J = 3.0 Hz), 2.59 (d, 1H, J = 3.0 Hz), 2.45 (d, 1H, J = 9.0 Hz), 2.42 (d, 1H, J = 9.0). ^{13}C NMR (500 MHz, D_2O, 25°C, δ): 180.14, 178.80, 140.58, 134.41, 130.46, 128.48, 127.30, 126.42, 66.27, 58.70, 58.57, 56.68.

Scheme S1. Synthesis of the Ligand

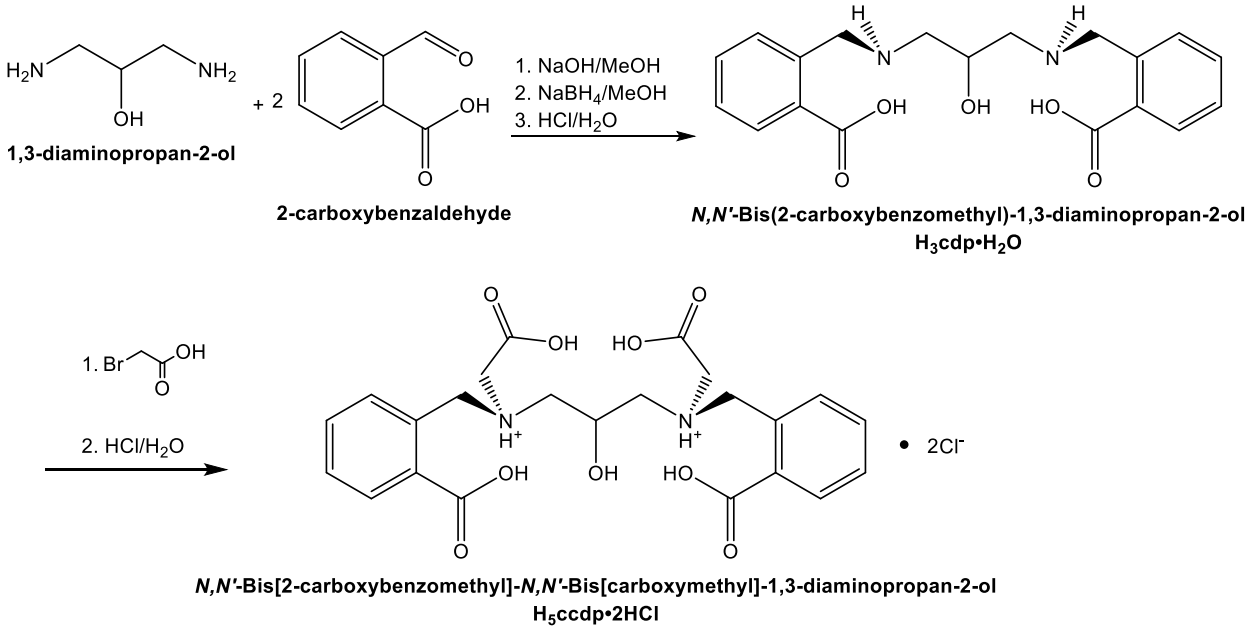

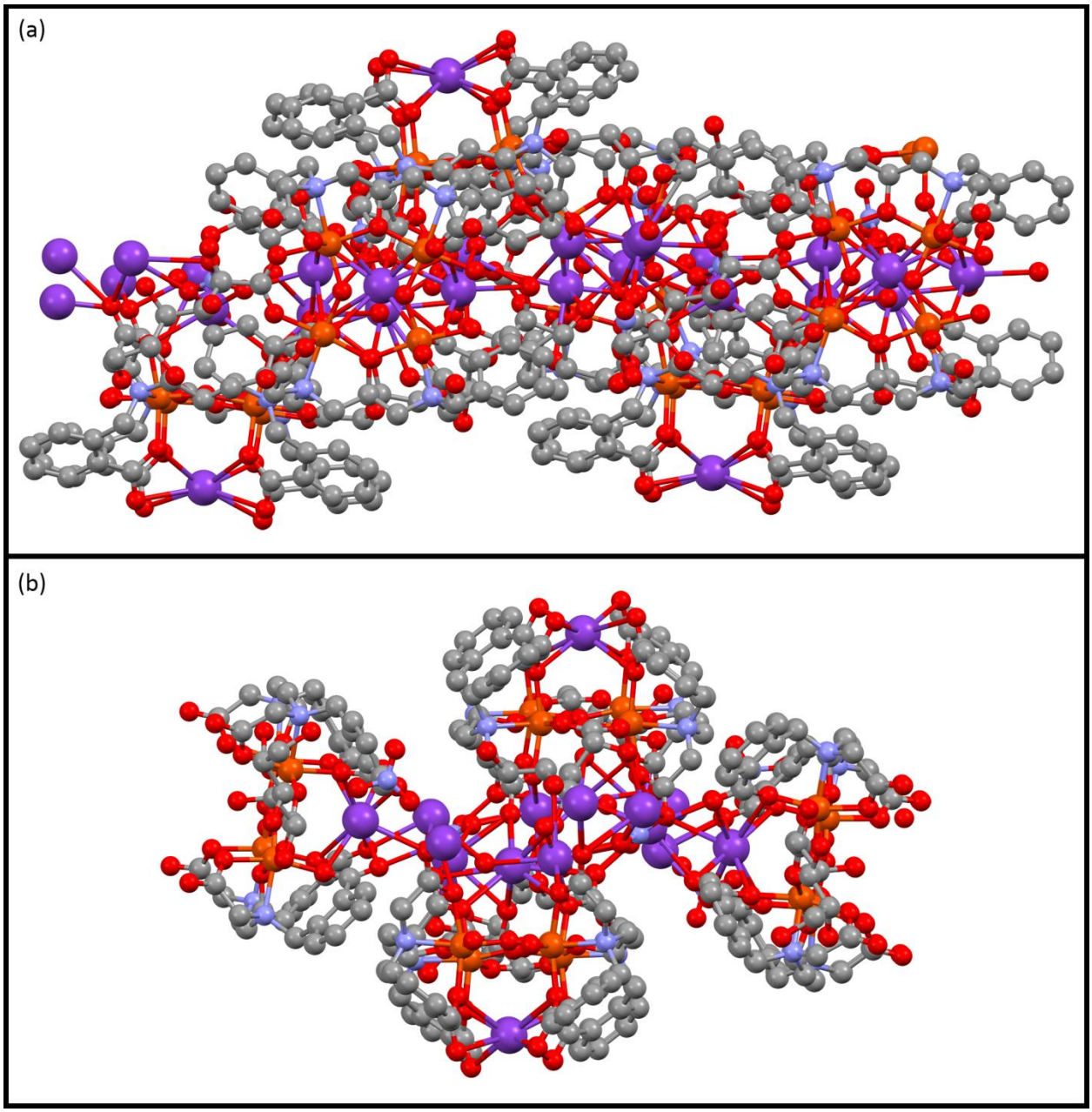

Fig. S1. Packing diagram of K_6[**1**]·$(NO_3)_3$·$10H_2O$ viewing from different angles, via the *c*-axis (a) and *a*-axis (b) showing potassium ion (in purple spheres) channel within the crystal lattice.

Table S1. Crystal Data and Structure Refinement for $K_6[1]\cdot(NO_3)_3\cdot 10H_2O$[a]

Empirical formula	$C_{116}H_{120}Fe_8K_{11}N_{12}O_{87.60}$
Formula weight	3960.73
Crystal system	orthorhombic
Space group	$P\ 2_12_12_1$
a, Å	19.4006(8)
b, Å	19.7985(7)
c, Å	22.1693(15)
α, deg	90.00
β, deg	90.00
γ, deg	90.00
vol., $Å^3$	8515.29
Z	2
$D_{(cal)}$, g/cm^3	1.537
$\mu(M_o\text{-}K_\alpha.mm^{-1})$	1.302
F(000)	3995.6
2θ range for data collection (^{0})	3.18 to 25.50
Index Ranges	$-23\leq h \geq 23$, $-23\leq k \geq 23$,
Reflections collected	$-26\leq l \geq 26$
Independent reflections	26293
Max. and Min. transmission	14737[R_{int} = 0.0265]
Data/Restraints/Parameters	1.000, 0.396
wR (F^2 all data)	14737/1105/0
R (*F* obsd data) [$I > 2\sigma(I)$]	R1 = 0.0793, wR2 = 0.1540
goodness-of-fit on F^2	R1 = 0.0603, wR2 = 0.1521
largest diff. peak and hole, e $Å^{-3}$	1.018 2.38/ -3.26

[a] $wR2 = \{\Sigma[w[F_o^2 - F_c^2)^2]/\ \Sigma[w(F_o^2)^2]\}^{1/2}$, $R1 = \Sigma||\ F_o| - |\ F_c||/\ \Sigma|\ F_o|$.

Table S2. Selected Bond Lengths and Angles in $K_6[1]\cdot(NO_3)_3\cdot10H_2O$

$K_6[1]\cdot(NO_3)_3\cdot10H_2O$			
Bond Lengths [Å]			
Fe(1) – O(19)	1.860(4)	Fe(2) – O(8)	1.977(4)
Fe(1) – O(5)	2.032(4)	Fe(2) – O(20)	1.867(4)
Fe(1) – O(1)	1.978(4)	Fe(2) – O(5)	2.023(4)
Fe(1) – O(4)	2.036(4)	Fe(2) – O(29)	2.030(4)
Fe(1) – N(1)	2.210(5)	Fe(2) – O(6)	2.047(4)
Fe(1) – O(22)	2.062(4)	Fe(2) – N(2)	2.230(6)
Fe(3) – O(19)	1.845(4)	Fe(4) – O(28)	2.050(4)
Fe(3) – O(17)	1.986(4)	Fe(4) – O(12)	2.040(4)
Fe(3) – O(14)	2.016(4)	Fe(4) – O(10)	1.978(4)
Fe(3) – O(15)	2.050(4)	Fe(4) – O(20)	1.870(4)
Fe(3) – N(4)	2.202(6)	Fe(4) – O(14)	2.028(4)
Fe(3) – O(21)	2.030(4)	Fe(4) – N(3)	2.218(5)
Bond Angles [deg]			
O(19) – Fe(1) – O(5)	93.6(2)	O(8) – Fe(2) – O(20)	101.4(2)
O(19) – Fe(1) – O(1)	101.0(2)	O(8) – Fe(2) – O(5)	89.9(2)
O(19) – Fe(1) – O(4)	94.4(2)	O(8) – Fe(2) – O(29)	91.0(2)
O(19) – Fe(1) – N(1)	169.1(2)	O(8) – Fe(2) – O(6)	162.3(2)
O(19) – Fe(1) – O(22)	94.1(2)	O(8) – Fe(2) – N(2)	87.7(2)
O(5) – Fe(1) – O(1)	88.7(2)	O(20) – Fe(2) – O(5)	91.6(2)
O(5) – Fe(1) – O(4)	92.8(2)	O(20) – Fe(2) – O(29)	93.0(2)
O(5) – Fe(1) – N(1)	82.5(2)	O(20) – Fe(2) – O(6)	96.0(2)
O(5) – Fe(1) – O(22)	172.0(2)	O(20) – Fe(2) – N(2)	169.1(2)
O(1) – Fe(1) – O(4)	164.4(2)	O(5) – Fe(2) – O(29)	175.0(2)
O(1) – Fe(1) – N(1)	89.1(2)	O(5) – Fe(2) – O(6)	93.1(2)
O(1) – Fe(1) – O(22)	92.1(2)	O(5) – Fe(2) – N(2)	82.2(2)
O(4) – Fe(1) – N(1)	75.8(2)	O(29) – Fe(2) – O(6)	84.5(2)
O(4) – Fe(1) – O(22)	84.3(2)	O(29) – Fe(2) – N(2)	93.0(2)
O(20) – Fe(1) – N(1)	89.5(2)	O(6) – Fe(2) – N(2)	75.5(2)
O(19) – Fe(3) – O(17)	102.1(2)	O(28) – Fe(4) – O(12)	83.4(2)
O(19) – Fe(3) – O(14)	91.5(2)	O(28) – Fe(4) – O(10)	90.3(2)
O(19) – Fe(3) – O(15)	95.8(2)	O(28) – Fe(4) – O(20)	93.3(2)
O(19) – Fe(3) – N(4)	169.1(2)	O(28) – Fe(4) – O(14)	173.4(2)
O(19) – Fe(3) – O(21)	93.8(2)	O(28) – Fe(4) – N(3)	90.6(2)
O(17) – Fe(3) – O(14)	90.1(2)	O(12) – Fe(4) – O(10)	162.3(2)
O(17) – Fe(3) – O(15)	161.5(2)	O(12) – Fe(4) – O(20)	95.6(2)
O(17) – Fe(3) – N(4)	86.9(2)	O(12) – Fe(4) – O(14)	94.0(2)
O(17) – Fe(3) – O(21)	89.8(2)	O(12) – Fe(4) – N(3)	76.3(2)
O(14) – Fe(3) – O(15)	94.0(2)	O(10) – Fe(4) – O(20)	101.3(2)
O(14) – Fe(3) – N(4)	82.2(2)	O(10) – Fe(4) – O(14)	90.4(2)
O(14) – Fe(3) – O(21)	174.6(2)	O(10) – Fe(4) – N(3)	87.2(2)
O(15) – Fe(3) – N(4)	75.8(2)	O(20) – Fe(4) – O(14)	92.9(2)
O(15) – Fe(3) – O(21)	84.4(2)	O(20) – Fe(4) – N(3)	170.6(2)
N(4) – Fe(3) – O(21)	92.3(2)	O(14) – Fe(4) – N(3)	83.0(2)

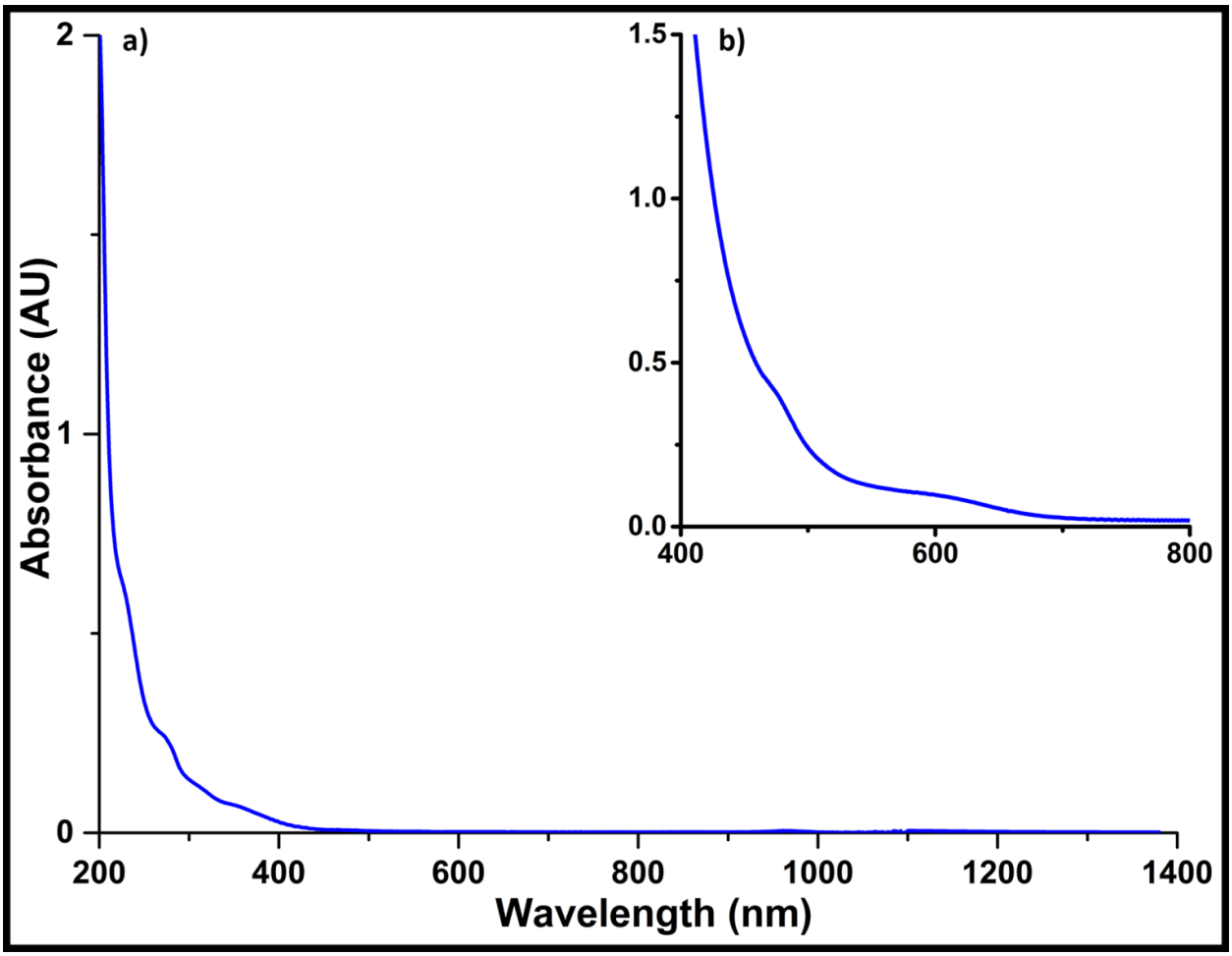

Fig. S2. UV-Vis spectra of 0.1 mM (a) and 5.0 mM (b) aqueous solutions of K_6[**1**]·$(NO_3)_3$·$10H_2O$ at 25 ºC.

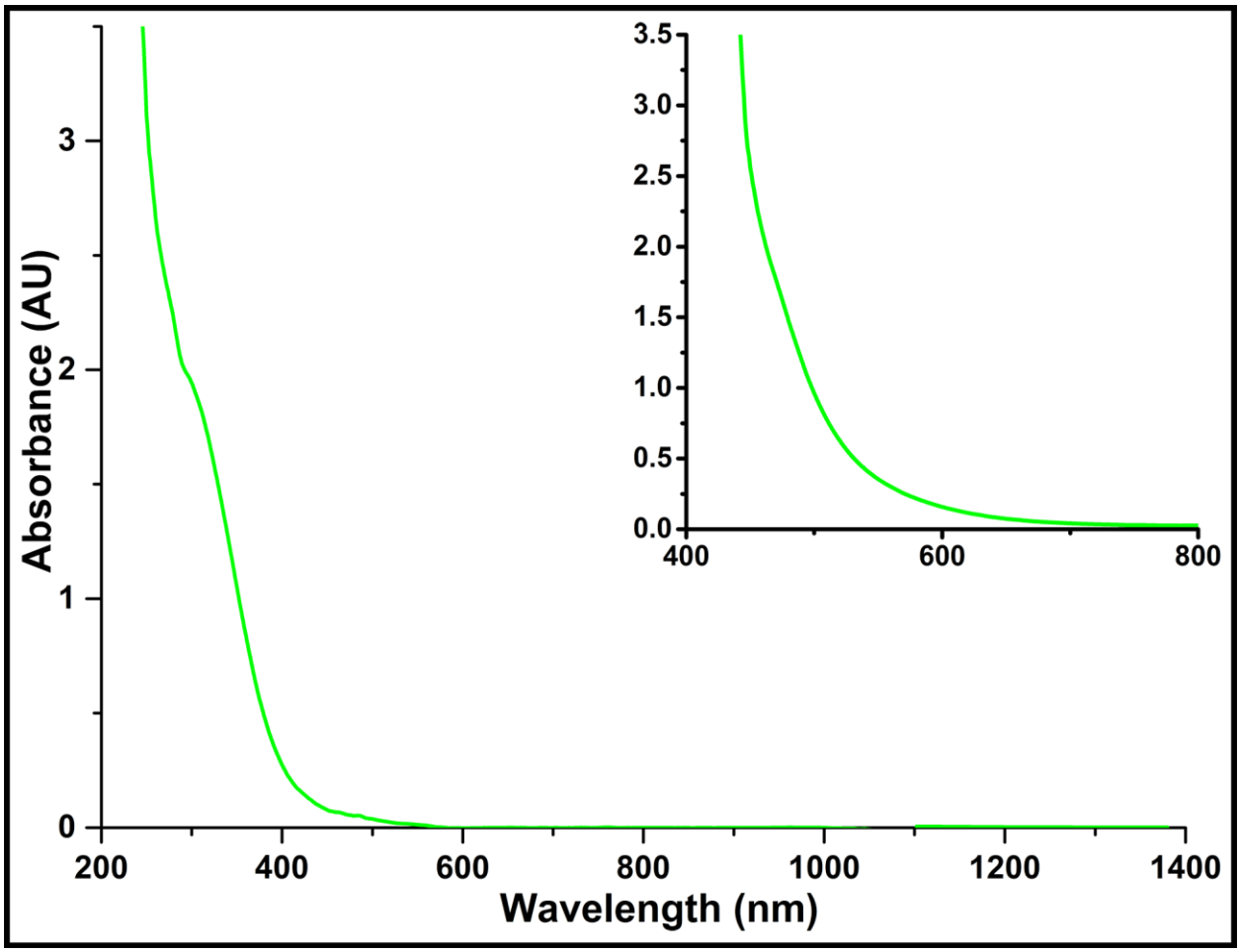

Fig. S3. UV-Vis spectra of 0.1 mM (a) and 5.0 mM (b) methanol solutions of K_6[**1**]·$(NO_3)_3$·$10H_2O$ at 25 ºC.

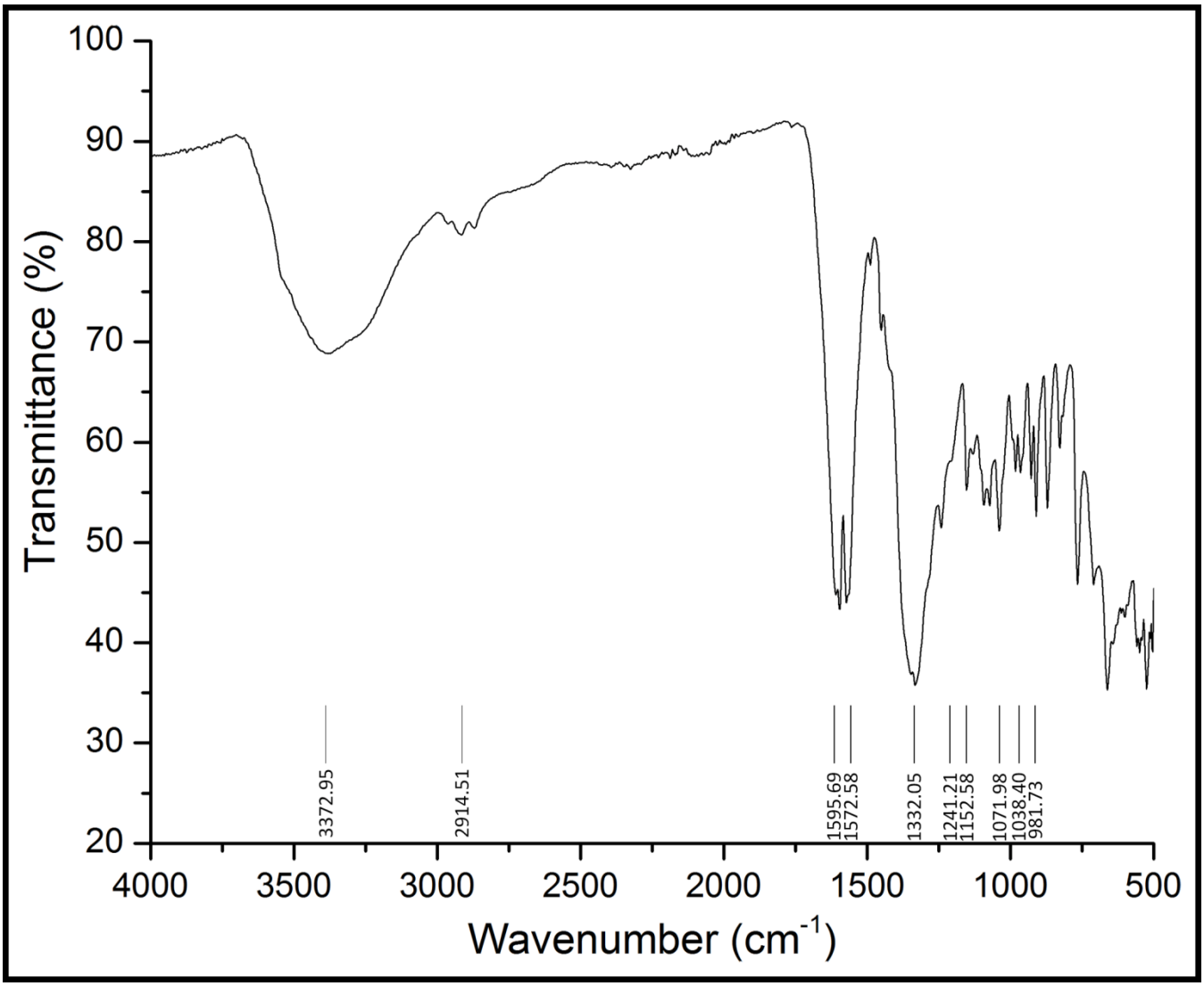

Fig. S4. FT-IR spectra of a powdered sample of K_6[**1**]·$(NO_3)_3$·$10H_2O$.

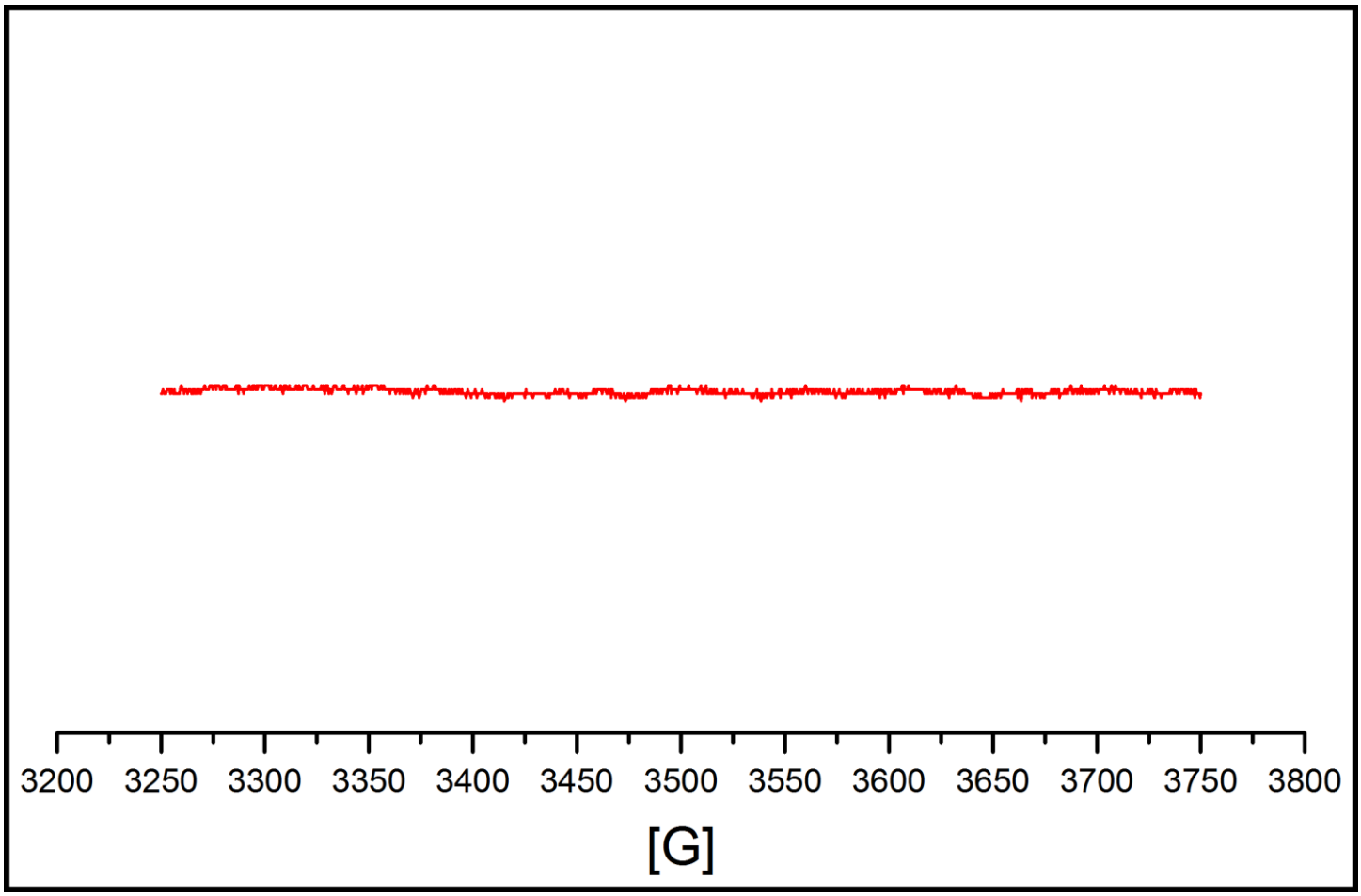

Fig. S5. X-band EPR spectrum of a powder sample of complex K_6[**1**]·$(NO_3)_3$·$10H_2O$ measured at room temperature.

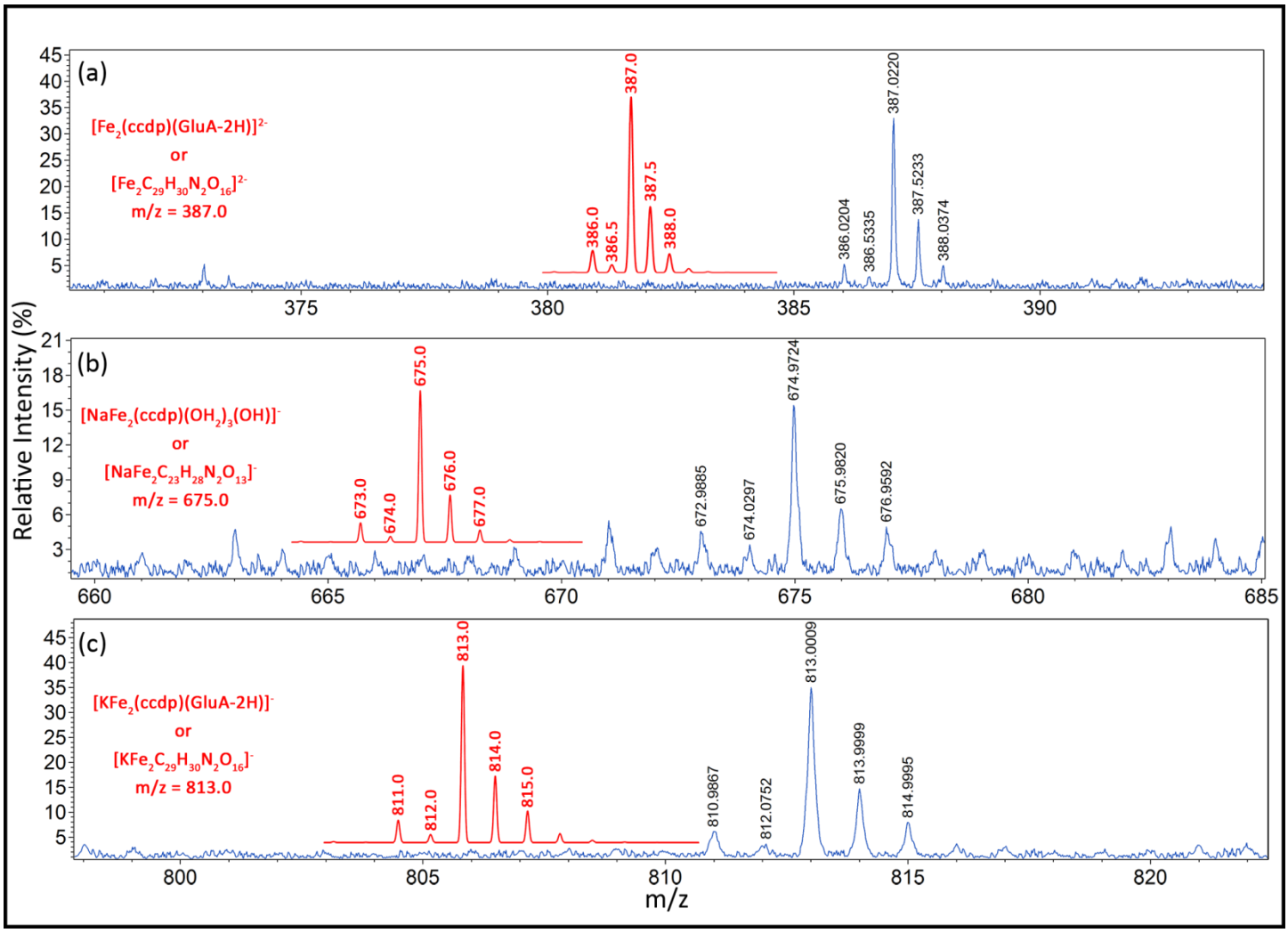

Fig. S6. Negative ion mode ESI-MS spectrum of 1 mg/mL aqueous solution of K_6[**1**]·$(NO_3)_3$·$10H_2O$; with the expanded regions to show the isotope distribution patters (shown in red is a simulated pattern) for *m/z* = 387 $[Fe_2C_{29}H_{30}N_2O_{16}]^-$ (a); *m/z* = 675 $[NaFe_2C_{23}H_{28}N_2O_{13}]^-$ (b); and *m/z* = 813 $[KFe_2C_{29}H_{30}N_2O_{16}]^-$ (c). Simulated isotope distribution patterns generated using Molecular Weight Calculator (Matthew Monroe, PNNL, Richland WA, U.S.A.) for the fragments.

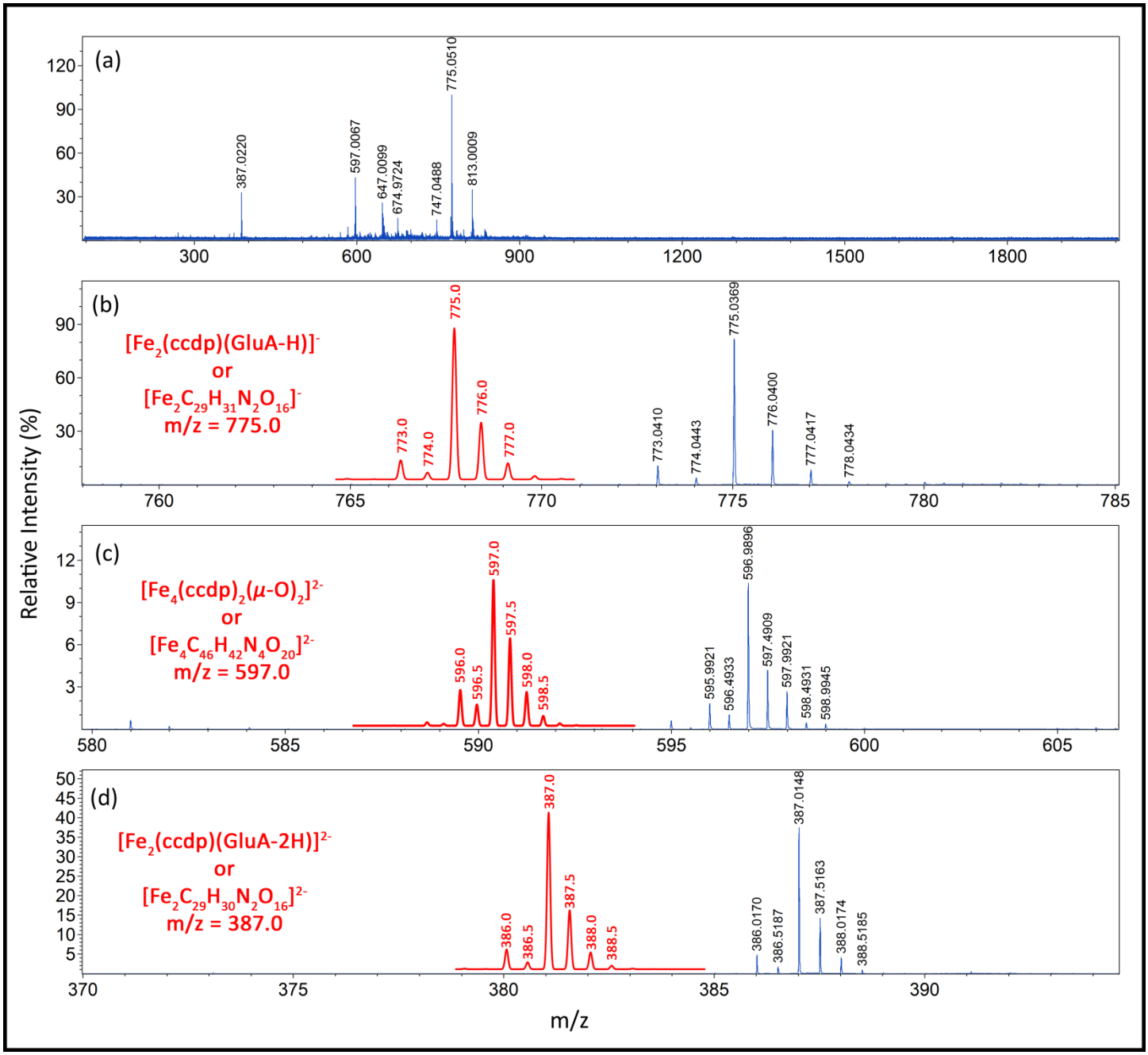

Fig. S7. Negative ion mode ESI-MS spectrum of 1 mg/mL methanolic solution of K_6[**1**]·$(NO_3)_3$·$10H_2O$; with the expanded regions to show the isotope distribution patters (shown in red is a simulated pattern) for *m/z* = 775 $[Fe_2C_{29}H_{31}N_2O_{16}]^-$ (a); *m/z* = 597 $[Fe_4C_{46}H_{42}N_4O_{20}]^{2-}$ (b); and *m/z* = 387 $[Fe_2C_{29}H_{30}N_2O_{16}]^{2-}$ (c). Simulated isotope distribution patterns generated using Molecular Weight Calculator (Matthew Monroe, PNNL, Richland WA, U.S.A.) for the fragments.

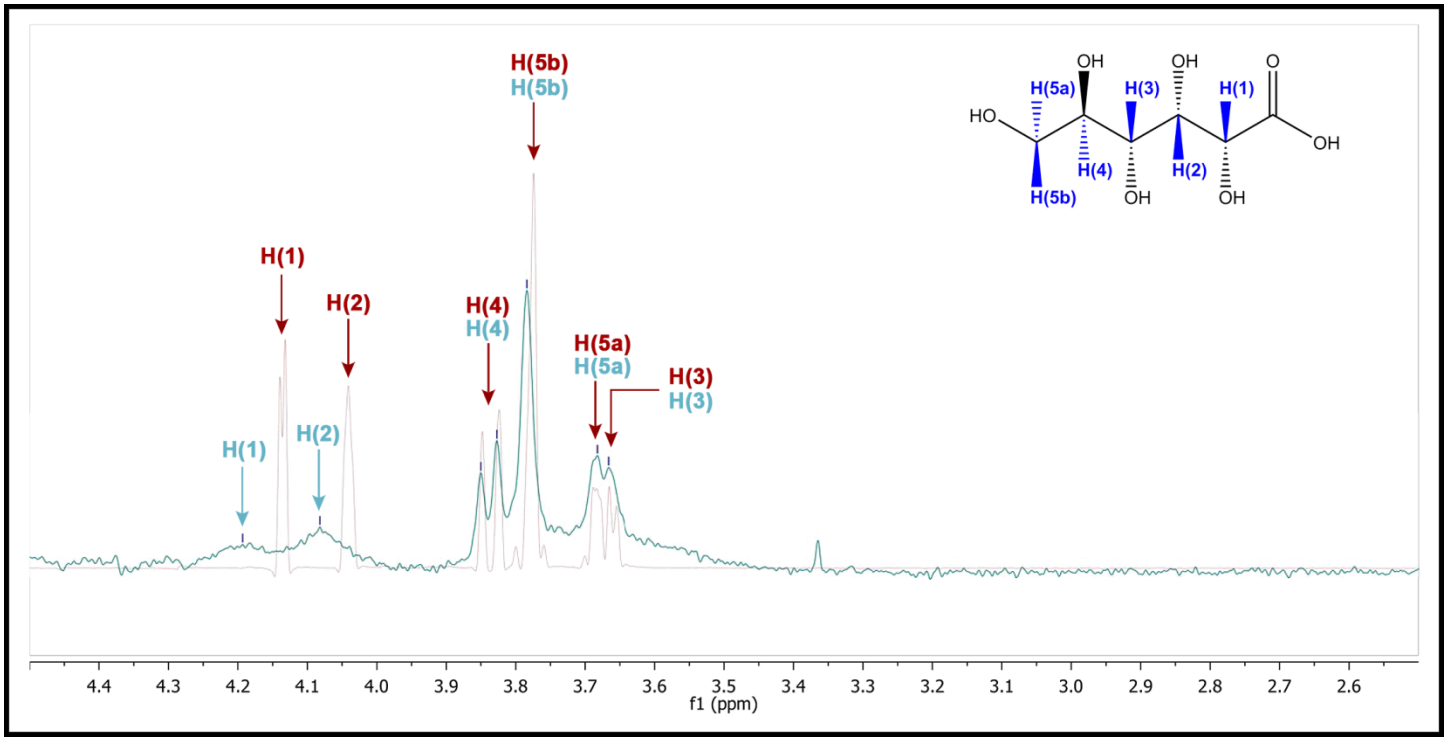

Fig. S8. Overlaid ^{1}H NMR spectrum in D_2O (0.10 mM) of $KC_6H_{11}O_7$ (shown in red) and K_6[**1**]·$(NO_3)_3$·$10H_2O$ (shown in blue) showing the up field shift of the H(1) and H(2) protons of the complex-bound gluconate ligands compared with the free gluconate ions. Peak broadening observed in the complex spectrum (shown in blue) due to the paramagnetic nature of K_6[**1**]·$(NO_3)_3$·$10H_2O$.

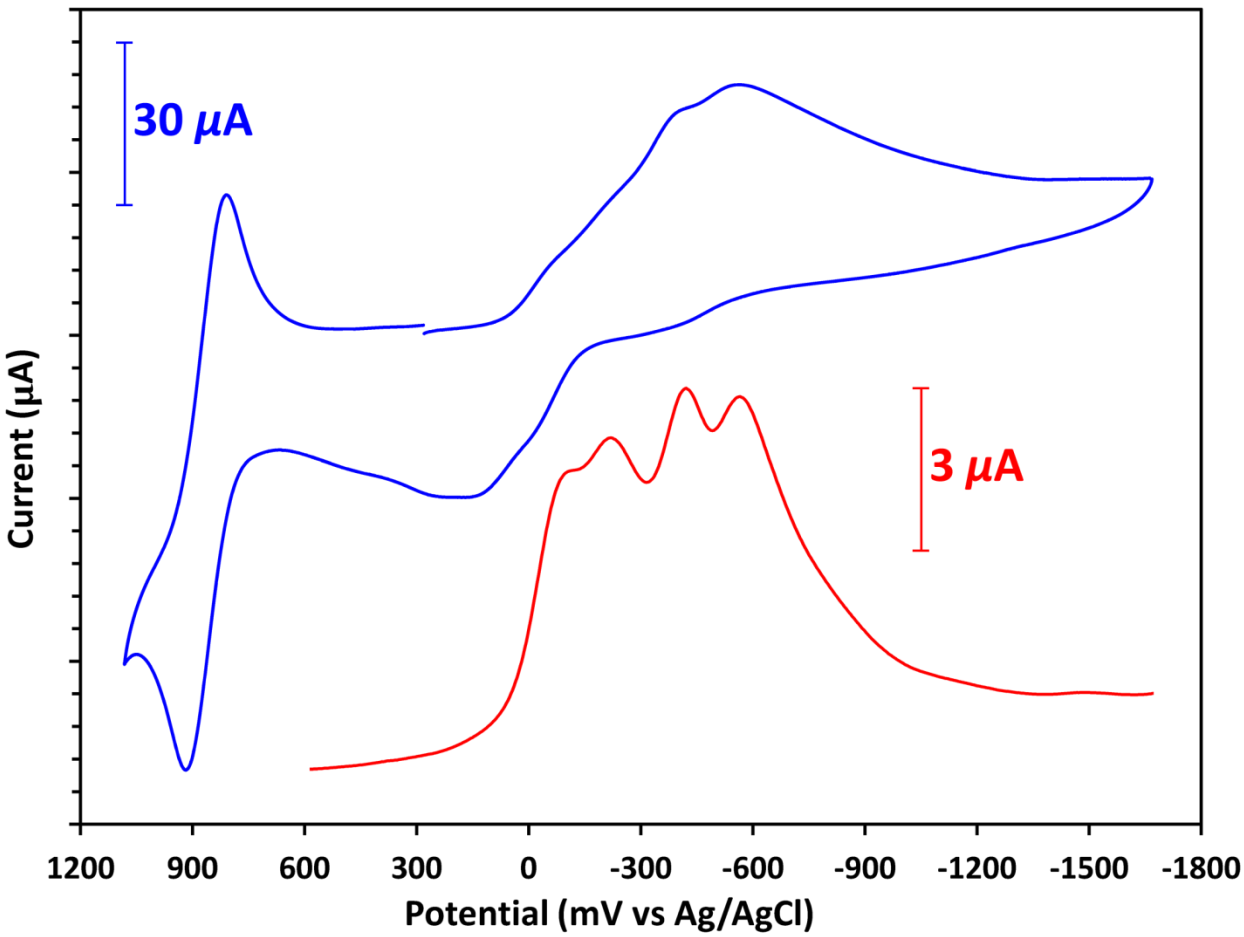

Fig. S9. Electrochemistry of 5.0 mM DMF solution of K_6[**1**]$(NO_3)_3 \cdot 10H_2O$ in 1.0 M TBAFP. (a) cyclic voltammogram with scan rate of 200 mV/s; and (b) square-wave voltammogram with 25 mV amplitude, 15 Hz frequency and E_{step} 4 mV using glassy carbon working electrode.

(a)

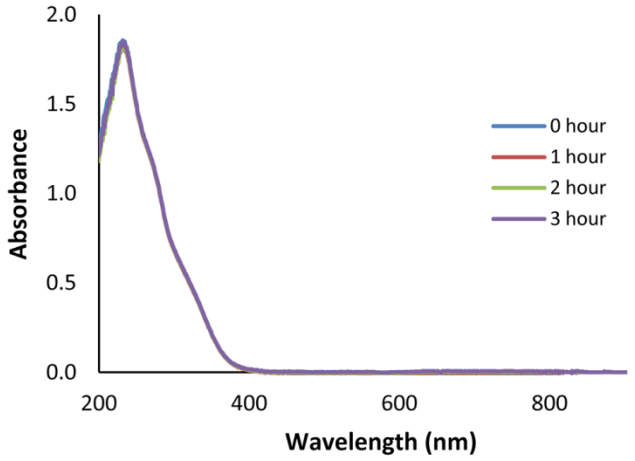
Absorbance
2.0
1.5
1.0
0.5
0.0
200
400
600
800
Wavelength (nm)
0 hour
1 hour
2 hour
3 hour

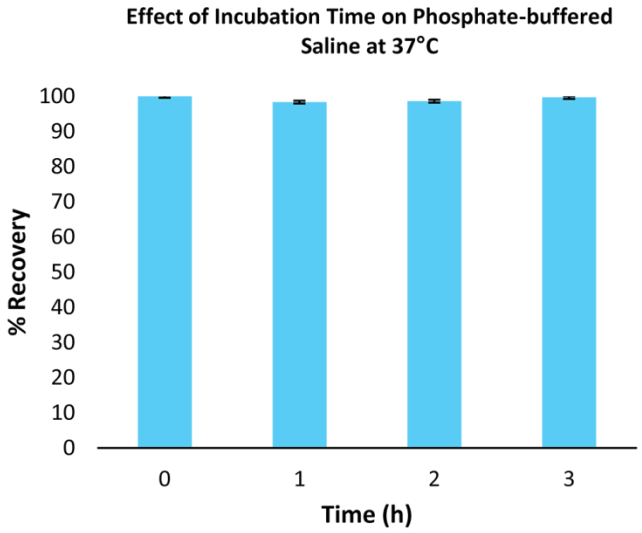
Effect of Incubation Time on Phosphate-buffered Saline at 37°C
% Recovery
100
90
80
70
60
50
40
30
20
10
0
0
1
2
3
Time (h)

(b)

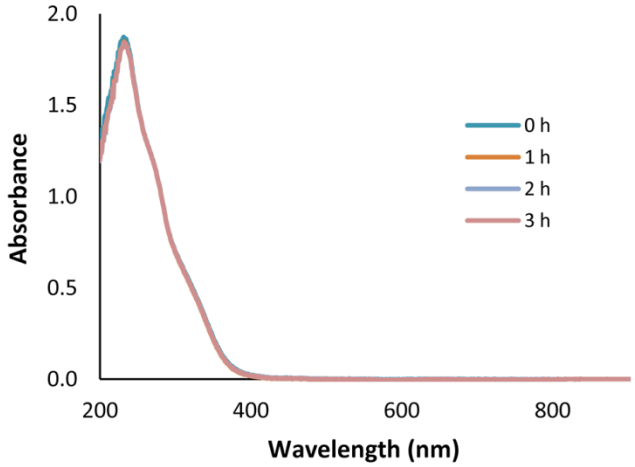
Absorbance
2.0
1.5
1.0
0.5
0.0
200
400
600
800
Wavelength (nm)
0 h
1 h
2 h
3 h

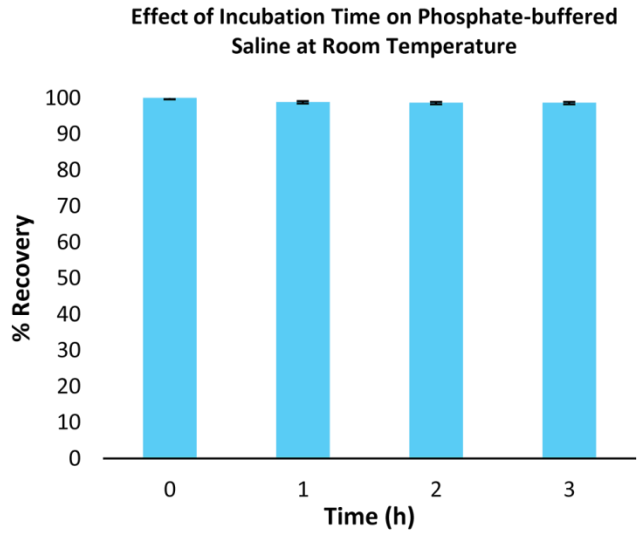
Effect of Incubation Time on Phosphate-buffered Saline at Room Temperature
% Recovery
100
90
80
70
60
50
40
30
20
10
0
0
1
2
3
Time (h)

(c)

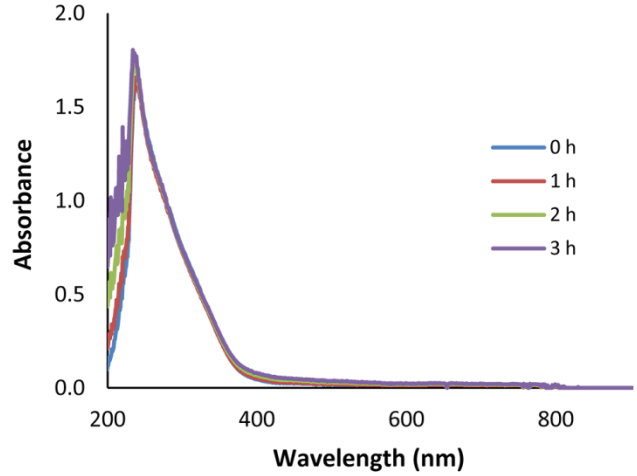
Absorbance
2.0
1.5
1.0
0.5
0.0
200
400
600
800
Wavelength (nm)
0 h
1 h
2 h
3 h

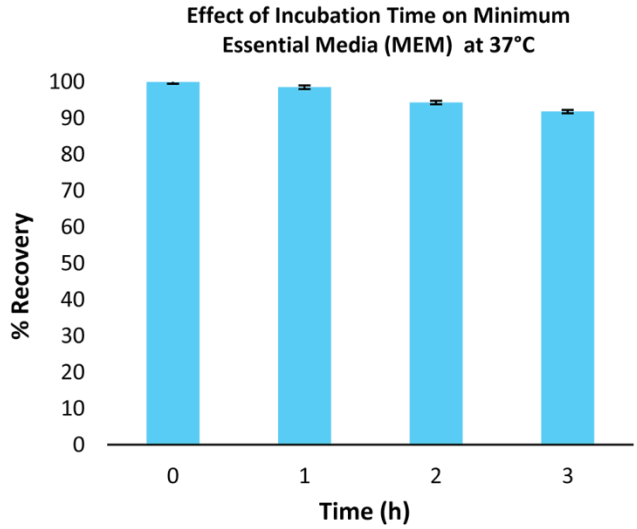
Effect of Incubation Time on Minimum Essential Media (MEM) at 37°C
% Recovery
100
90
80
70
60
50
40
30
20
10
0
0
1
2
3
Time (h)

(d)

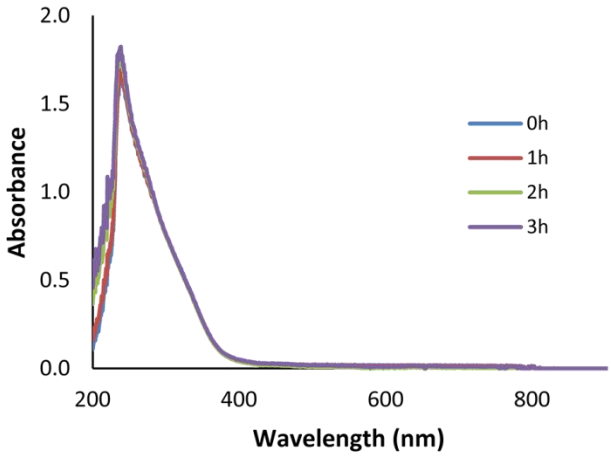
Absorbance
2.0
1.5
1.0
0.5
0.0
200
400
600
800
Wavelength (nm)
0h
1h
2h
3h

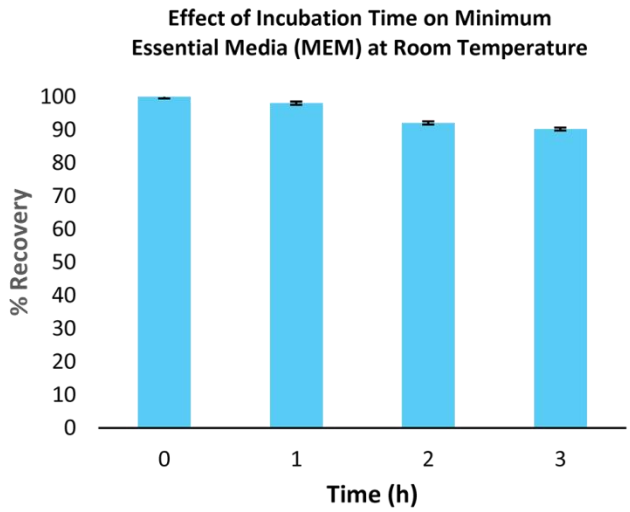
Effect of Incubation Time on Minimum Essential Media (MEM) at Room Temperature
% Recovery
100
90
80
70
60
50
40
30
20
10
0
0
1
2
3
Time (h)

(e)

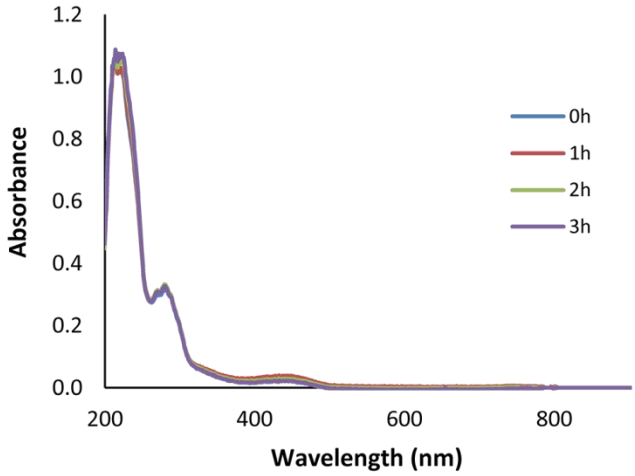
Absorbance
1.2
1.0
0.8
0.6
0.4
0.2
0.0
200
400
600
800
Wavelength (nm)
0h
1h
2h
3h

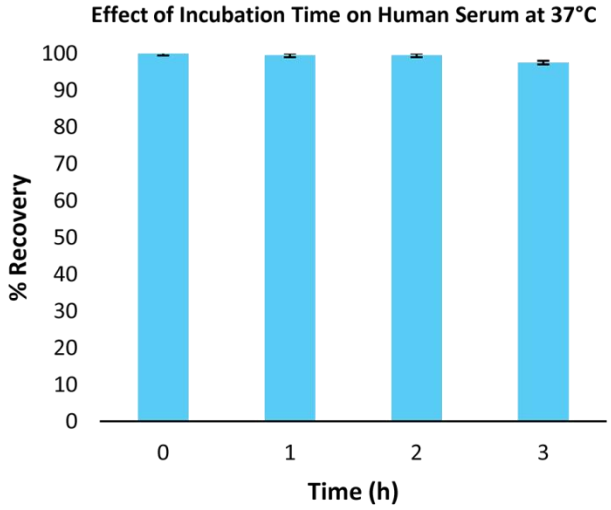
Effect of Incubation Time on Human Serum at 37°C
% Recovery
100
90
80
70
60
50
40
30
20
10
0
0
1
2
3
Time (h)

(f)

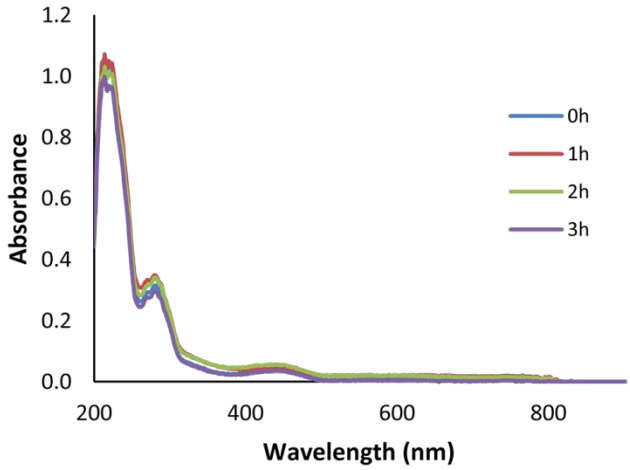
Absorbance
1.2
1.0
0.8
0.6
0.4
0.2
0.0
200
400
600
800
Wavelength (nm)
0h
1h
2h
3h

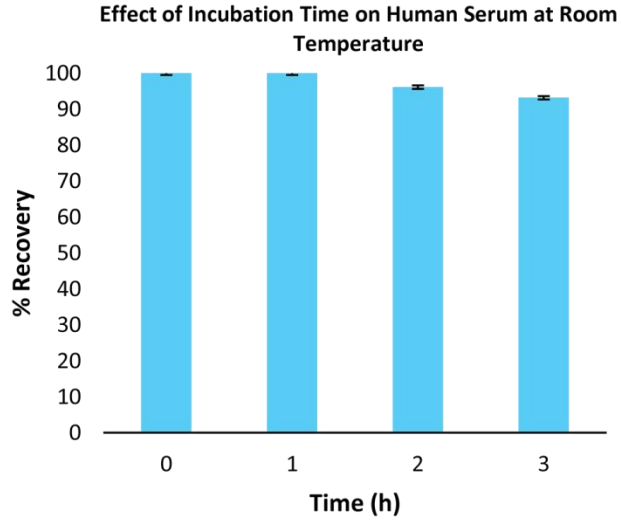
Effect of Incubation Time on Human Serum at Room Temperature
% Recovery
100
90
80
70
60
50
40
30
20
10
0
0
1
2
3
Time (h)

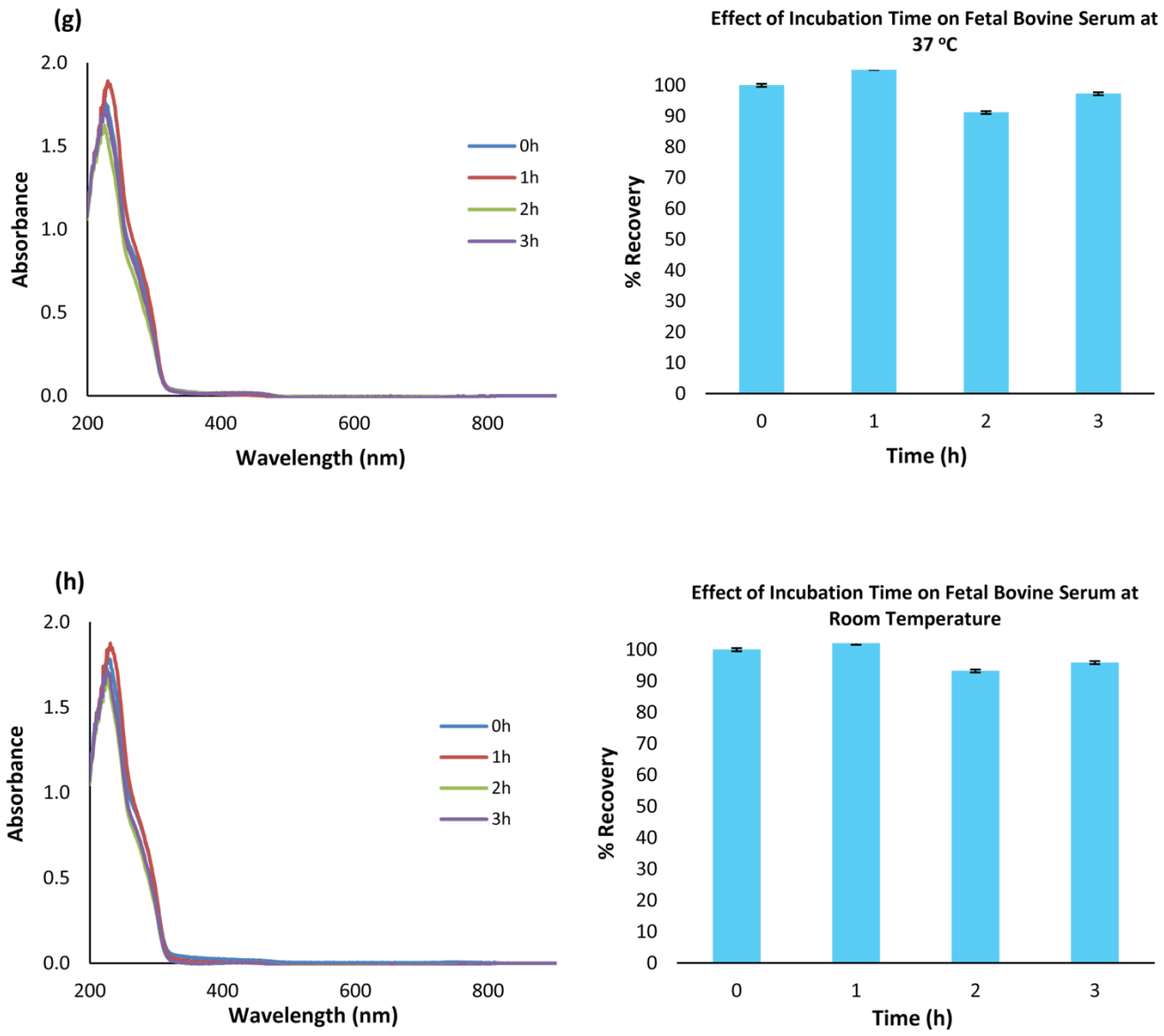

Fig S10. UV-Vis stability study and effect of incubation time of 50μM K_6[**1**]$(NO_3)_3 \cdot 10H_2O$ in Phosphate Buffer Saline at 37ºC (a), and room temperature (b); Minimum Essential Medium at 37ºC (c), and room temperature (d); Human Serum at 37 °C (e), and room temperature (f); Fetal Bovine Serum at 37 °C (g), and room temperature (h).